HPS/ECal simulations: energy and position reconstruction for electrons, positrons and photons

Holly Szumila-Vance (ODU) and Michel Garçon (JLab & CEA-Saclay)

July 24, 2014

Internal Note to the HPS collaboration

1 Introduction

After one of us (HSV) implemented the detailed ECal geometry and the clustering algorithm [1] into the GEANT-based HPS simulation software, SLIC, we turn here to the detailed study of the energy and position reconstruction in this calorimeter. We make use of previous experience with the CLAS/IC calorimeter [1, 2, 3], though there are significant differences between HPS/ECal and CLAS/IC. In our case, there is a wider spread of angles of incidence of particles (electrons, positrons and photons) with respect to the crystal orientation. Also, there will be more edge effects in the ECal. All of this will induce energy and position dependent (and particle dependent because of the magnetic field bending) corrections to the measured energy and position.

Denoting E_i the energy deposited in crystal i, smeared with a Gaussian distributed preamplifier noise, the cluster energy is

$$E_{cl} = \sum_i E_i, \tag{1}$$

where the sum runs over crystal energies above a given threshold, and the particle energy is

$$E = \frac{E_{cl}}{f}, \tag{2}$$

with f the sampling fraction to be determined. A precise determination of energy requires a precise simulation of f and equally precise calibration of the deposited energies E_i, and in turn any calibration based on the analysis of electromagnetic showers will rely on the knowledge of the sampling fraction.

In the end, an energy resolution comparable to the SVT momentum resolution is expected, thus contributing significantly to the final lepton pair invariant mass resolution.

As for position, it has been known for a long time (see [2] and references therein) that the most intuitive energy weighted average over crystal central positions results in an unphysical periodic position pattern with too large position spreads. After some trials, we adopt the same weighting scheme as in [2]:

$$x_{cl} = \frac{\sum_i w_i x_i}{\sum_i w_i}, \text{ with } w_i = \max\left[0, w_0 + \ln\frac{E_i}{E_{cl}}\right], \tag{3}$$

and similarly for the vertical position y_{cl}. The positive parameter w_0 acts as a relative energy threshold $E_i/E_{cl} > e^{-w_0}$, while the logarithmic weights favor the lateral tails of the shower for a more precise position determination. In addition, we expect a sizeable correction Δx due to the angle of incidence of the tracks upon the crystal (so called depth correction).

The position measurement is needed for calibration (or calibration checks) using $\pi^0 \to \gamma\gamma$ events and for track matching with the SVT information for (accidental) background reduction.

Δx and in a lesser extent f depend on the angle of incidence α (track angle with respect to the axis of the crystal at impact location), which in turn, for a point target, depends on ECal position and energy, as well as on the type of particles. The ranges of α values are illustrated in Fig. 1, while Fig. 2 gives for electrons the dependence of α on position at ECal front face and energy, which is governed by the magnet field and the crystal angles. Electrons cannot reach the last 8-9 cm to the left of ECal. For photons, α depends only on position. In all cases, the range of incident angles is significantly larger than for CLAS/IC (1 to 4°). In this Note, with the exception of Fig. 2, we consider particles within the ECal acceptance, which is somewhat larger than the SVT acceptance, in order to fully understand the ECal response.

Rather than expressing α as a function of position and energy, and then Δx and f as a function of α, we find it more practical (and logically strictly equivalent) to directly find the position and energy dependencies of Δx and f (and possibly w_0). Besides, there may be other energy dependence than through the angle of incidence, as the (albeit small) logarithmic dependence of the longitudinal shower development. This approach is even necessary when dealing with edge effects, where the angle of incidence is not the only relevant variable, or again if thresholds are not the same for all crystals.

2 Event generation and selection

Electrons, positrons and photons were generated at fixed energies at the HPS target point location. Tracking is performed in the 0.5 T magnetic field (constant field), corresponding to the run at 2.2 GeV beam energy. Any energy loss between the target and ECal front

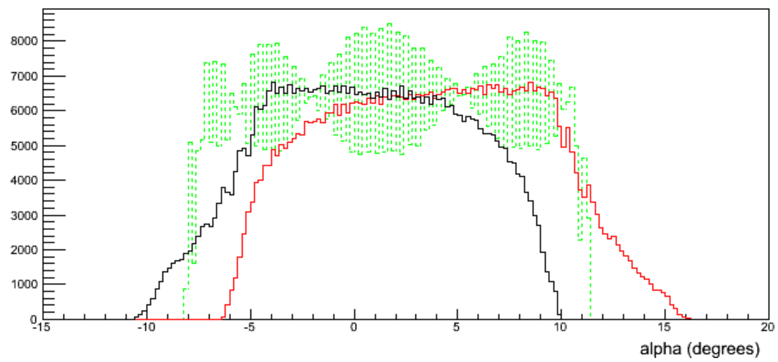

Figure 1: Angle of incidence α, for 0.4 to 2.2 GeV electrons (black), positrons (red) and photons (green) emitted in the horizontal plane at all angles accepted by ECal.

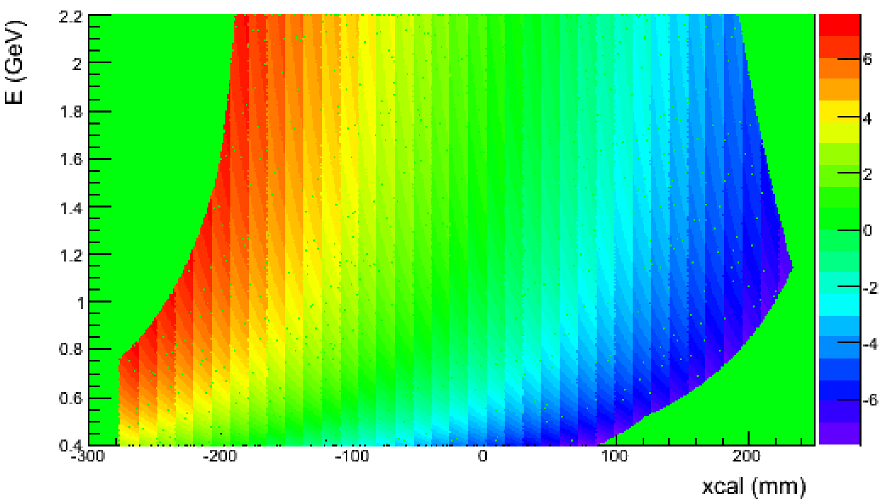

Figure 2: Angle of incidence α vs E and x, for electrons, with the condition that at least 4 SVT layers are hit.

face is neglected (which implies it is absorbed in the definition of the sampling fraction). Whenever more than one cluster is found (because of secondaries), the highest energy cluster is selected.

- Generated energies $E = 0.5, 0.75, 1, 1.25, 1.5, 2.5$ and 5 GeV (the two highest energies are inaccessible for the run at 2.2 GeV, but they are useful here to pin down the energy dependence of some parameters).

- Generated angles at target location: $\pm 16^\circ$ of target centerline
- Preamplifier noise added randomly to crystal energies (rms): 3 MeV.
- Crystal energy threshold: 7.5 MeV.
- Cluster seed energy threshold: 100 MeV.
- Cluster energy threshold: $E_{cl} > 300$ MeV.
- Track coordinates x_{gen} and y_{gen}, as well as crystal center coordinates x_i and y_i, defined on ECal front face: $z = 139.3$ cm from target.

3 Main features neglecting edge effects and some position dependencies

In this section, we exclude events where the generated position is within a border crystal. We also postpone the study of position dependence of f to concentrate on the main features of the calorimeter response.

3.1 Energy

3.1.1 Electrons

For 1 GeV electrons, the hit multiplicity is given in Fig. 3 and the cluster energy distribution in Fig. 4. A fit to the peak of this distribution yields the average energy resolution $\sigma_E/E = \sigma_{E_{cl}}/\langle E_{cl}\rangle$ and the average sampling fraction $\langle E_{cl}\rangle/E$. Note that we do not claim a precision better than 1% in this fit.

Compiling the results at different fixed energies, we get f as a function of E_{cl} and σ_E/E as a function of E (Figs 5 and 6). The (small) drop of f at low energy is attributed to the energy threshold per crystal. The fitted energy resolution is:

$$\frac{\sigma_E}{E}(\%) = \frac{1.60}{E} \oplus \frac{2.46}{\sqrt{E}} \oplus 1.51 \tag{4}$$

The first term corresponds to the preamplifier noise. We would have expected 3 MeV $\times\sqrt{10} = 0.009$ GeV, where 10 is the average number of hit crystals. The second term corresponds to statistical fluctuations in the shower development (lateral containment, energy deposited,...). The third term is interpreted as fluctuation of energy leakage from the back of the crystals. Should be added to it the crystal-to-crystal intercalibration error which we hope to maintain at the 1% level. We thus expect a $3.3\% \oplus 1\% = 3.5\%$ energy resolution at 1 GeV.

For an improved estimate of the energy resolution, one should also take into account the FADC errors and the fluctuations in the number of photons, but we do not expect

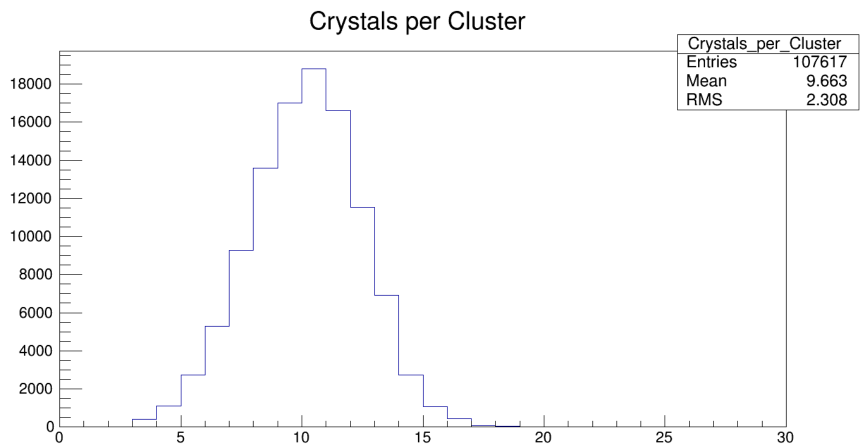

Figure 3: Hit multiplicity per cluster for $E = 1$ GeV electrons, summed over all positions.

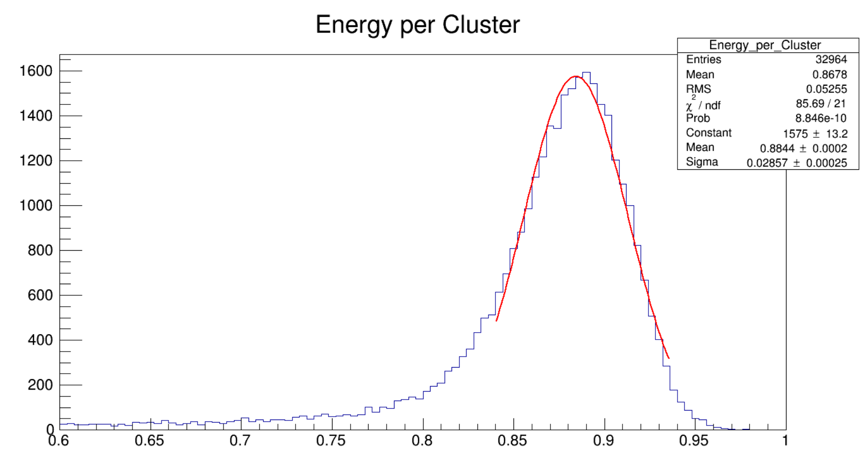

Figure 4: E_{cl} for $E = 1$ GeV electrons, summed over all positions, with gaussian fit on peak.

the numbers to change much. Ultimately, the resolution will be measured with elastically scattered electrons and with neutral pion decays.

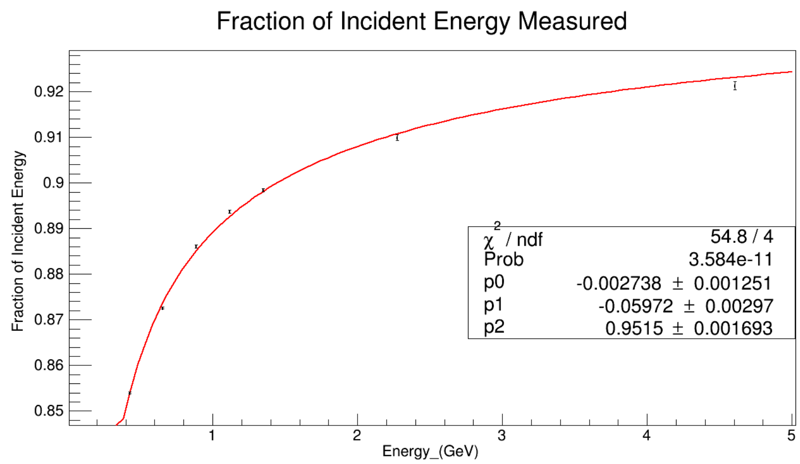

Figure 5: Sampling fraction f as a function of E_{cl}, for electrons.

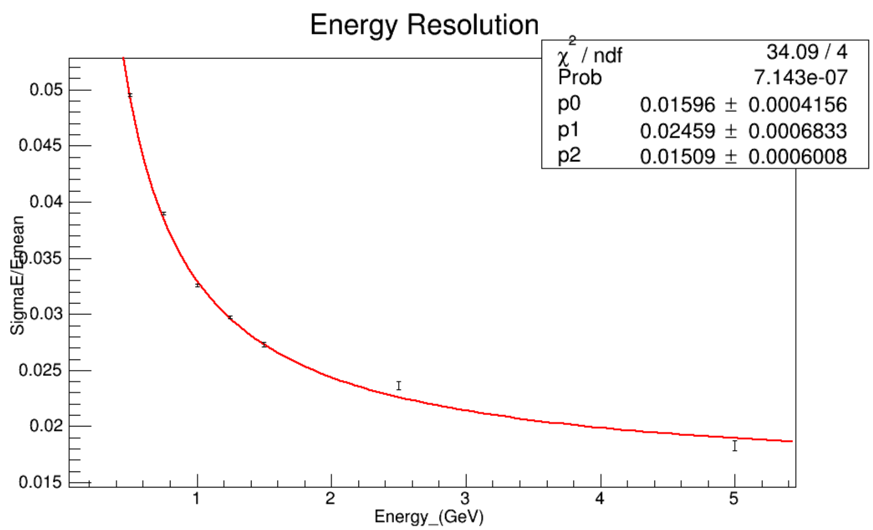

Figure 6: σ_E/E as a function of E for electrons, together with fit according to Eq. 4

3.2 Positrons

As expected, the sampling fraction (Fig. 7) and energy resolution (Fig. 8) for the positrons are very similar to the results of the previous subsection for electrons.

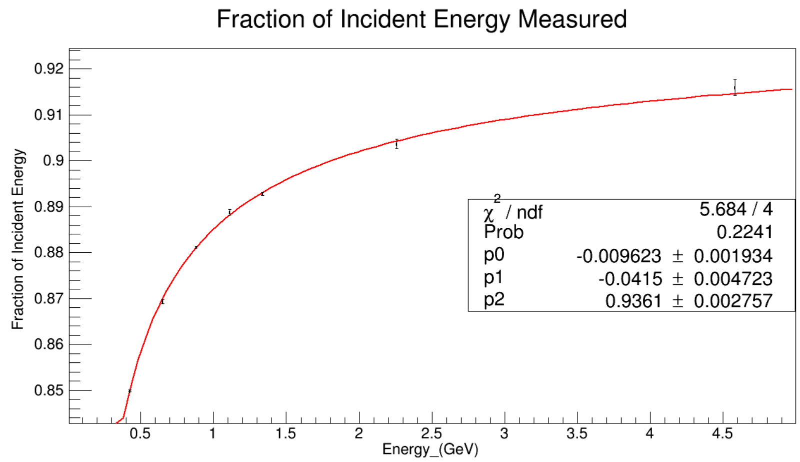

Figure 7: Sampling fraction f as a function of E_{cl}, for positrons.

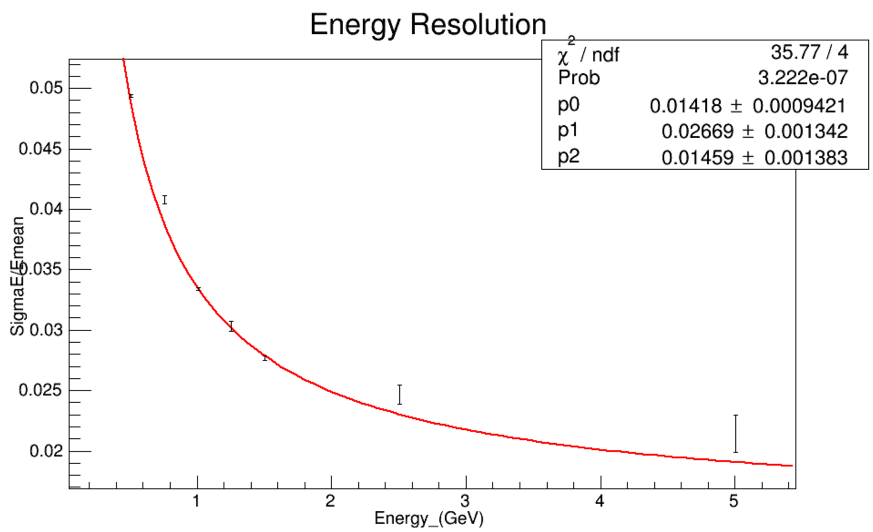

Figure 8: σ_E/E as a function of E for positrons, together with fit according to Eq. 4

3.2.1 Photons

For photons as well, we find very similar results, as shown in Figs 9 and 10.

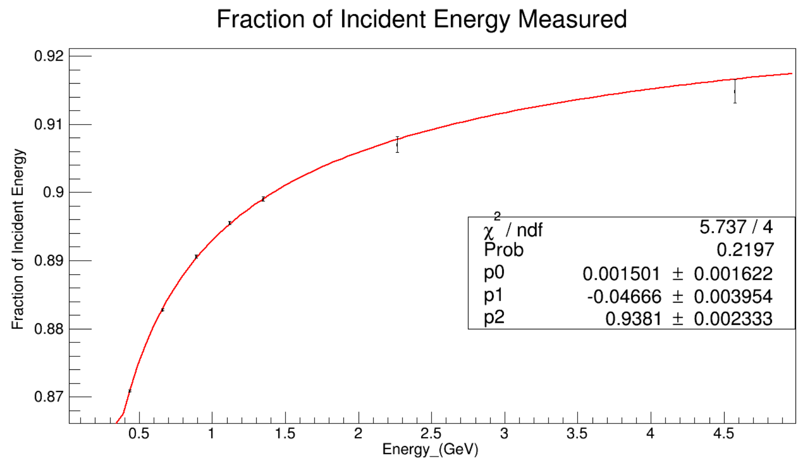

Figure 9: Sampling fraction f as a function of E_{cl}, for photons.

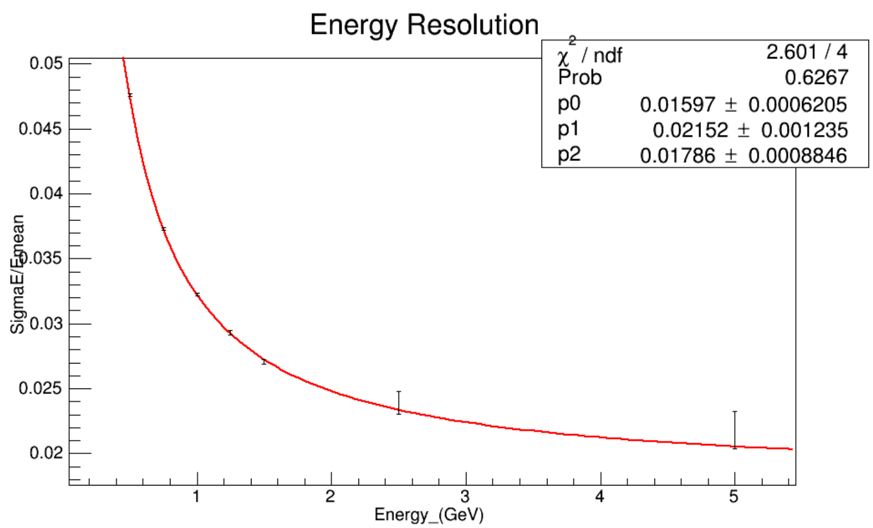

Figure 10: σ_E/E as a function of E for photons, together with fit according to Eq. 4

3.3 Position

The impact position on the front face of the calorimeter is first calculated according to Eq. 3. An optimization of the parameter w_0 yields a value of $w_0 = 3.1$, almost energy independent, close to the one adopted in Ref. [2] The plots of $x_{cl} - x_{gen}$ vs x_{gen} hereafter show on one hand an unavoidable residual oscillation with a periodicity equal to the crystal size, and on the other hand a position dependent offset due to the longitudinal development of the shower along an axis different from the crystal axis at that particular position. The x-offset has a linear dependence so that we end up with a corrected position:

$$x = x_{cl} - A_{part}(E_{cl})x_{cl} - B_{part}(E_{cl}), \quad \text{with } part = e^-, e^+, \gamma, \tag{5}$$

while we find no need for a correction in $y = y_{cl}$.

From the 1D histogram of $x - x_{gen}$, we get the position resolution σ_x which then plotted as a function of energy and parameterized as

$$\sigma_x = \frac{p_0}{\sqrt{E}} + p_1 \tag{6}$$

A position resolution better than 2 mm in both x and y is found for 1 GeV particles. This resolution improves with higher energies. At this level of resolution, the ECal position information could be used as an additional constraint in the SVT track fitting algorithm, thus improving (ever so slightly) the resulting momentum resolution.

3.3.1 Electrons

The minimization of the position resolution with respect to the parameter w_0 (Fig. 11) yields the optimal value of 3.1. This value only changes very slightly at higher energies, so that the value at 1 GeV energies was selected for all position studies hereafter.

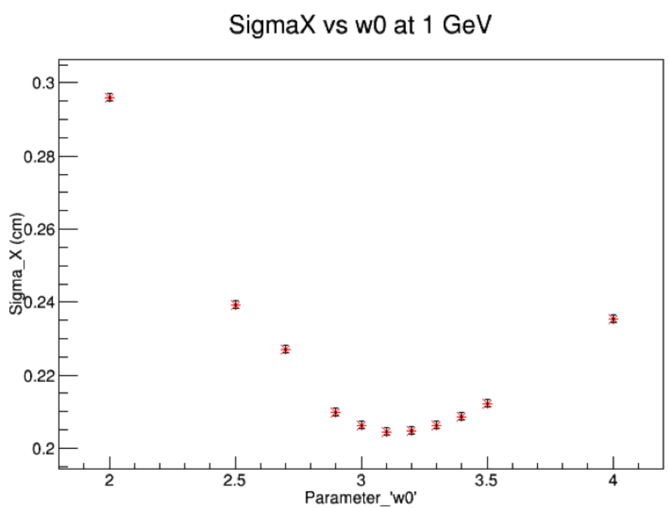

Figure 11: σ_x as a function of w_0 for 1 GeV electrons.

The position reconstruction according to Eq. 3 is shown in Fig. 12. The straight line fit allows us to obtain the correction factor added in Eq. 5 . The final result is shown in Fig. 13.

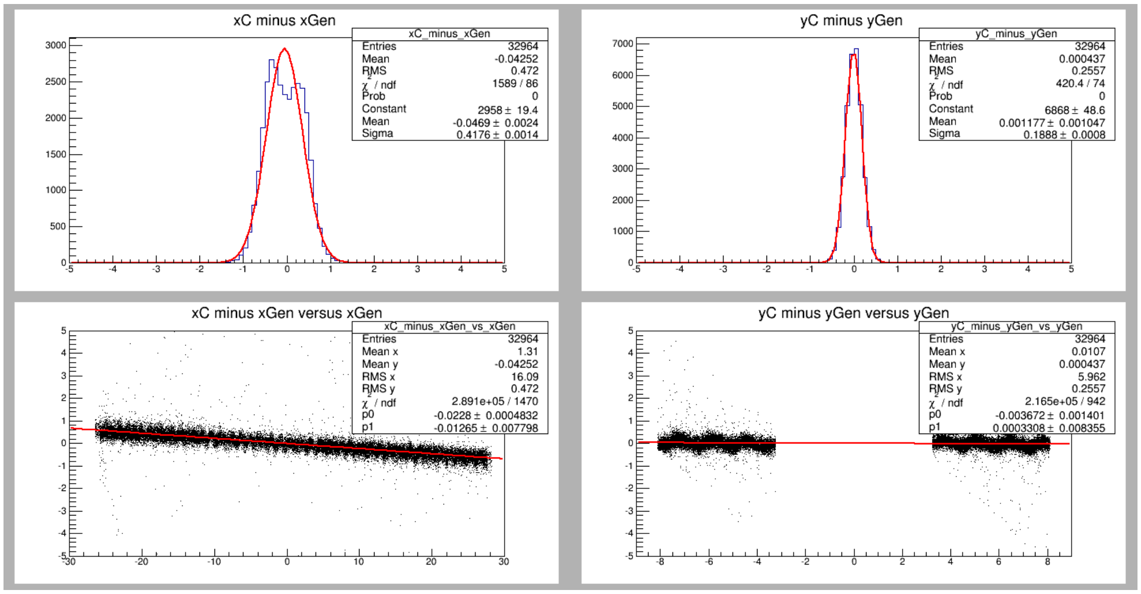

Figure 12: Position reconstruction for 1 GeV electrons, before correction.

In order to implement the correction factor for different energies, the coefficients of A and B are shown in Fig. 14.

3.3.2 Positrons

The same analysis conducted for electrons was used to investigate the position dependencies and resolution for positrons. The same w_0 value for electrons is found to be useful in the weighting scheme for calculating the position centroid of a cluster from positrons as shown in Fig. 16.

Additionally, the same method for correcting the positions for positrons is shown in Figs. 17 and 18.

The dependency of the variables A and B on the cluster energy are very similar to that of the electrons with B being opposite in curvature as shown in Fig. 19.

3.3.3 Photons

Using the weighting value where $w_0 = 3.1$, the photon position corrections were calculated using the same procedure as for the electrons and positrons (Figs. **??**, **??**, **??** and 24). The

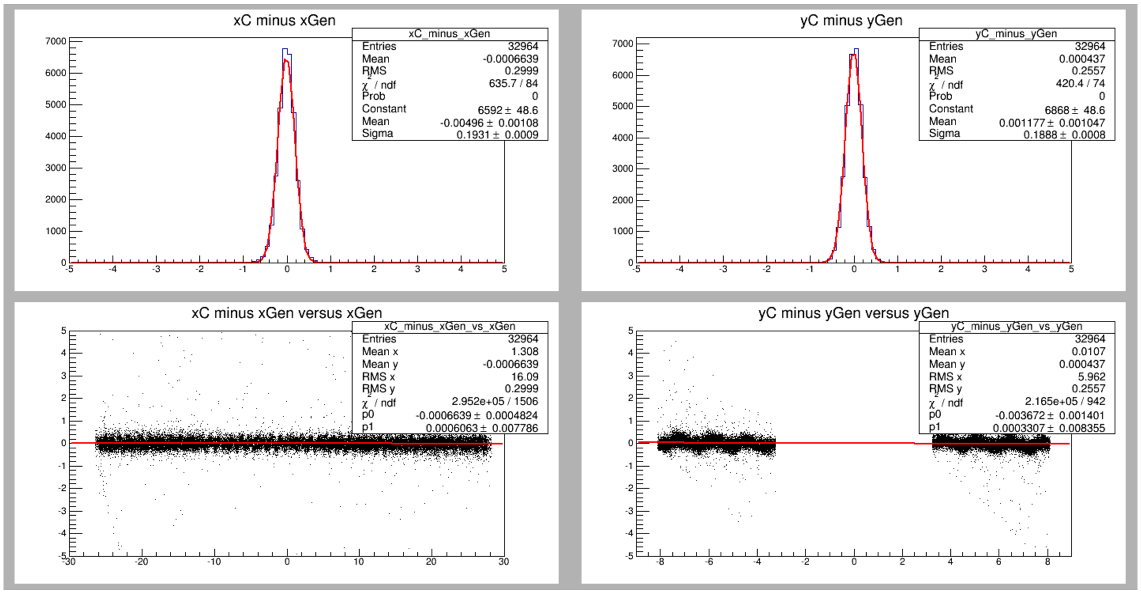

Figure 13: Position reconstruction for 1 GeV electrons, after correction.

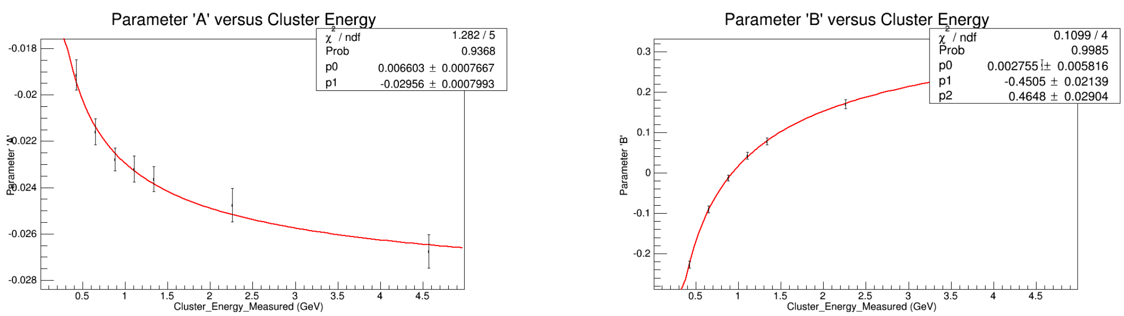

Figure 14: A and B position correction parameters for electrons.

A slope parameter is slightly shifted compared to electrons and photons, while B varies much less with energy (see change of vertical scale).

4 Edge effects

A preliminary study of the edge effects serves as a criterion for determining how reliably we can reconstruct an event occurring near the edge of the ECal. Due to symmetrical results, we confine the presentation of the results of our study to events occurring in the top half

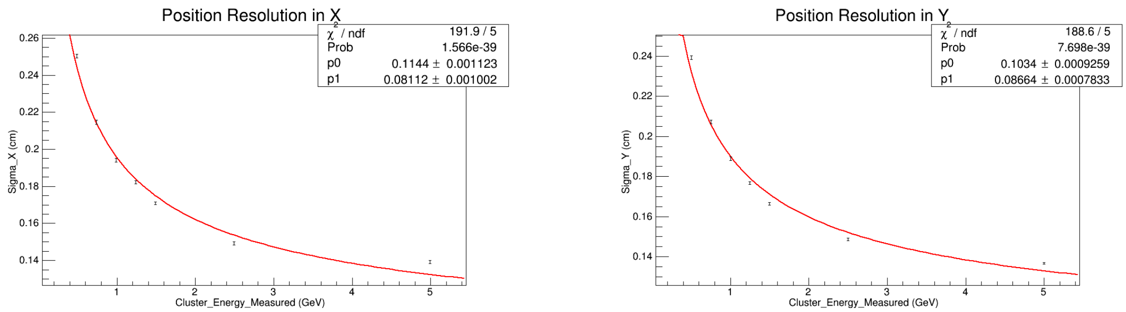

Figure 15: Position resolutions σ_x and σ_y for electrons (as a function of E).

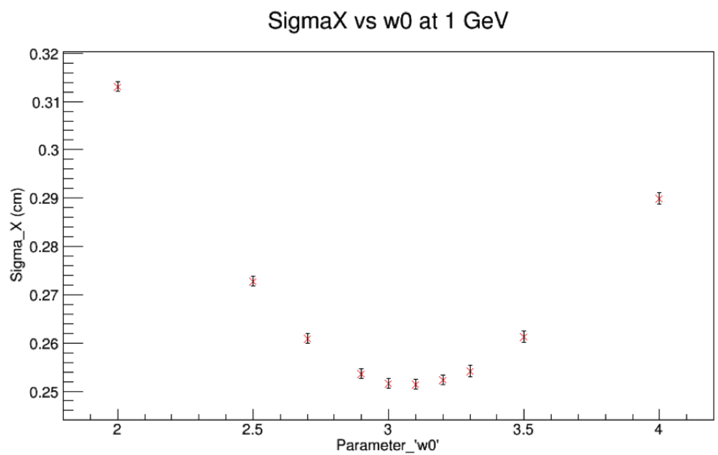

Figure 16: σ_x as a function of w_0 for 1 GeV positrons.

of the ECal. There are two primary edge effects of interest. The first type of edge includes the edges along the top, bottom, and center of the ECal. The second type of edge includes edges along the far left and right sides of the ECal that are primarily occupied by particles most affected by the magnetic field (in the case of positrons and electrons).

For 1 GeV electrons, we take vertical slices throughout the ECal (fixing the x-location) and study the sampling fraction as a function of vertical position in these regions. The result of this study is shown in Fig. 25. We observe that the sampling fraction holds fairly constant, within 1-2%, until approximately 1 cm of the edge (3/4 of the crystal dimension) where we begin to see a rapid deterioration of the energy deposited. These results are consistent with the findings for the IC [2].

We obtain similar results for 1 GeV photons incident on the ECal (Fig. 26). Both results confirm that hits occurring up to 1 cm from the edge of a crystal can be safely

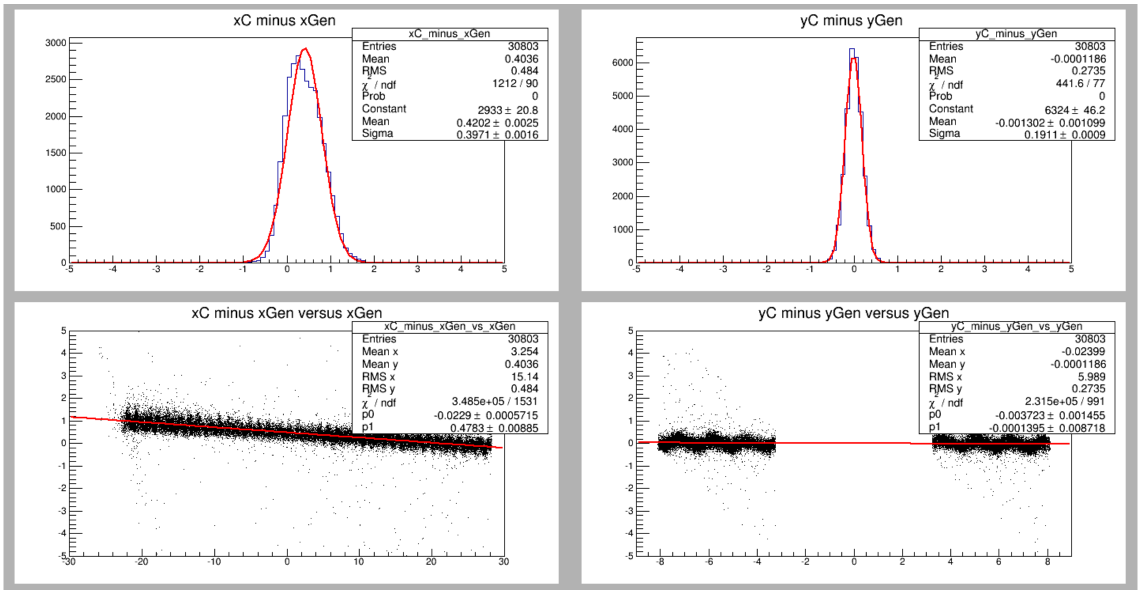

Figure 17: Position reconstruction for 1 GeV positrons, before correction.

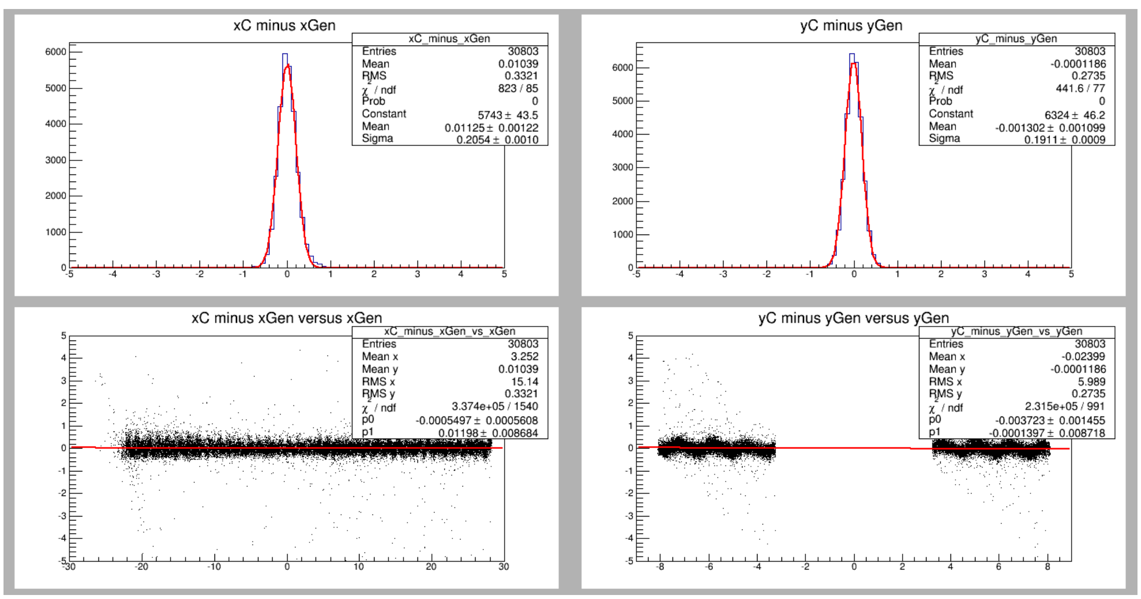

Figure 18: Position reconstruction for 1 GeV positrons, after correction.

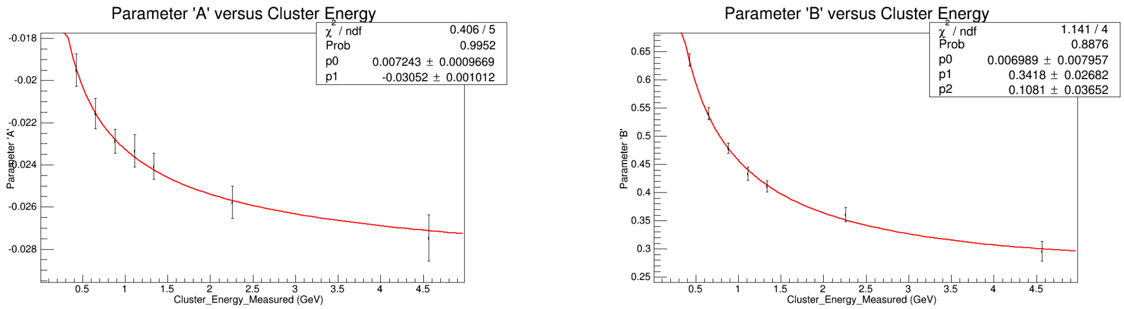

Figure 19: A and B position correction parameters for positrons.

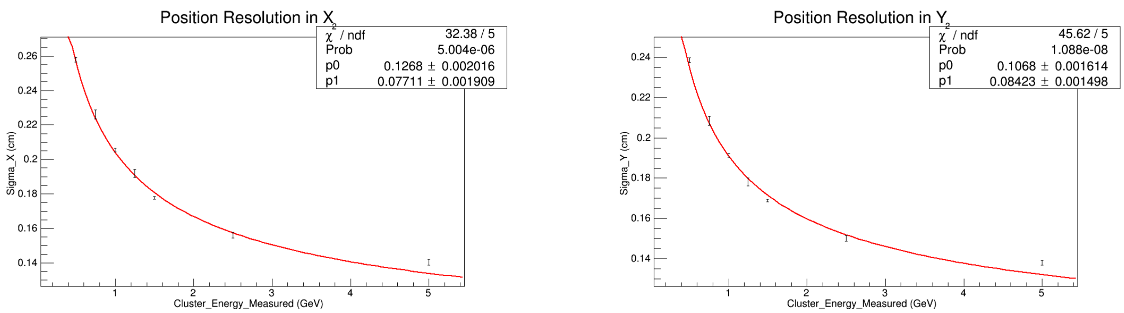

Figure 20: Position resolutions σ_x and σ_y for positrons (as a function of E).

reconstructed.

The side (vertical) edges were studied by fixing a narrow range of y and then observing the reconstructed energy fraction toward the edge. The results for electrons are shown in Fig. 27. The edge effect is more significant at lower energy (slightly less than 1 cm at 1 GeV, and more than 1 cm at 0.5 GeV). These results are consistent with positrons on the other half of the ECal.

Additionally, the position reconstruction is an important consideration with respect to the edges. If the position reconstruction is still reliable near the edges of the ECal, further studies may be able to attain corrected energy fits for specific regions close to the edges in order to increase statistics. These studies would be best accomplished in conjunction with calibration studies.

The results of the position reconstruction on the top edge and the edge along the center of the ECal are shown in Figs. 28 and 29. For Fig. 28 where the limits in x are fixed, we observe a similar position deterioration to that of the energy (approximately 0.75 of the crystal face or about 1 cm). However, when we fix the limits in y to study the outside edges of the ECal as in Fig. **??**, the results indicate that position reconstruction may

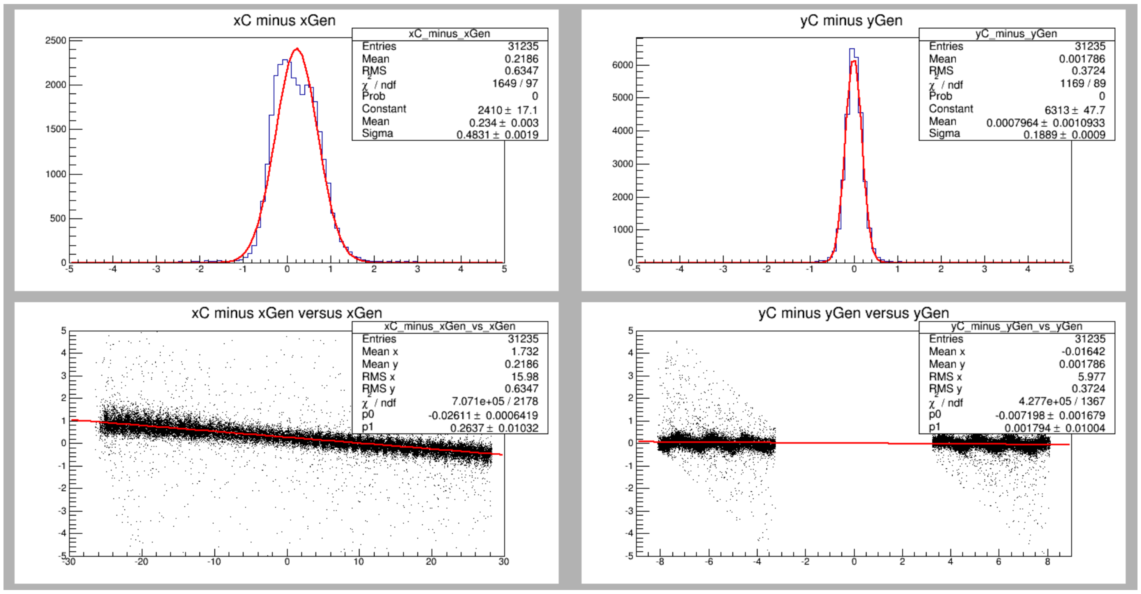

Figure 21: Position reconstruction for 1 GeV photons, before correction.

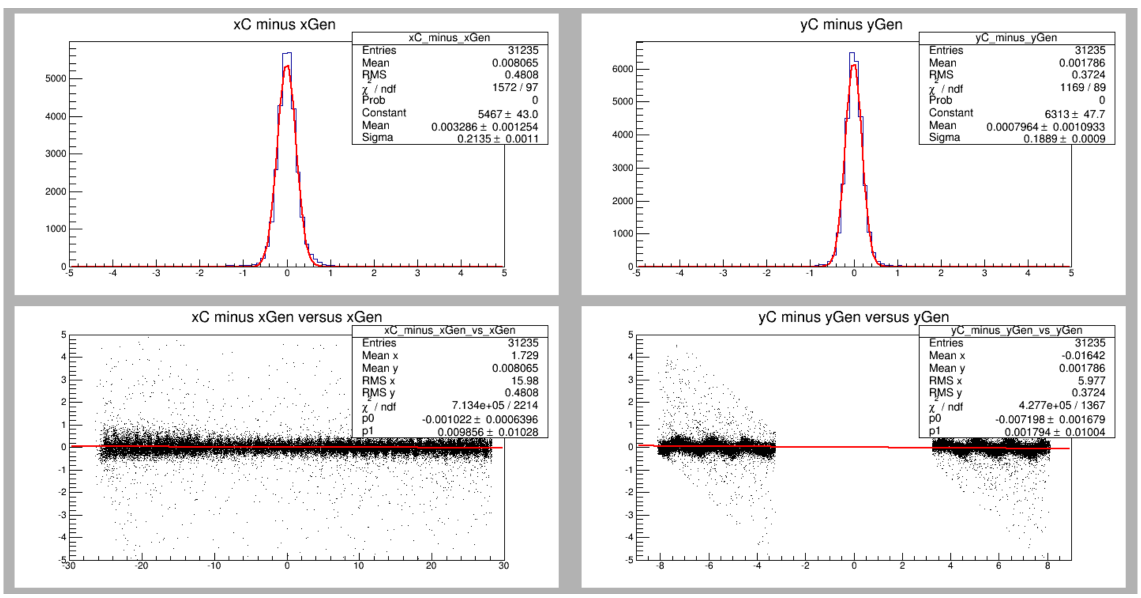

Figure 22: Position reconstruction for 1 GeV photons, after correction.

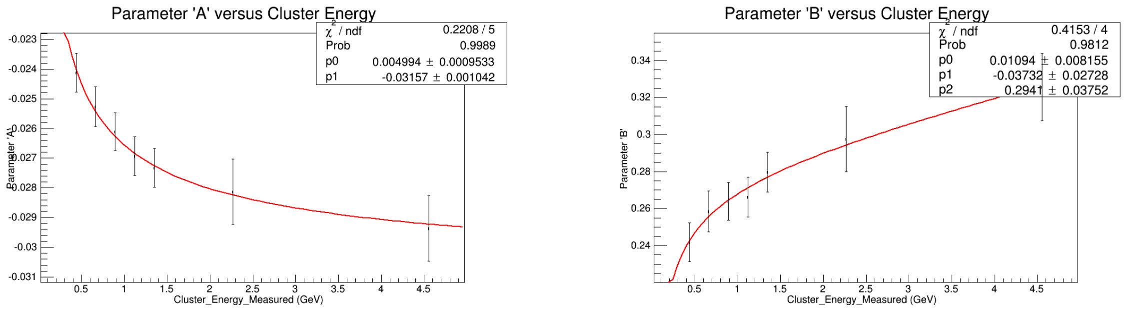

Figure 23: A and B position correction parameters for photons.

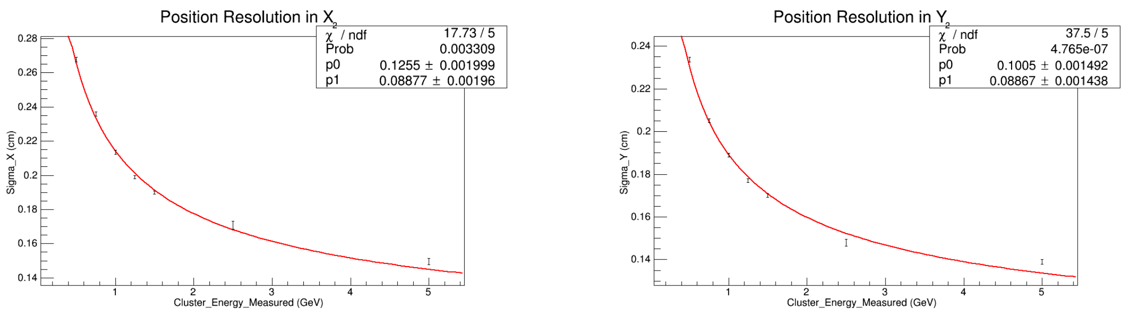

Figure 24: Position resolutions σ_x and σ_y for photons (as a function of E).

allow a further extrapolation into the outer edge crystals in order to attain more statistics. Edge effects causing a deterioration of position reconstruction at the outer (left and right) edges of the ECal appear to decrease with higher energies. For 0.5 GeV electrons, we see approximately 1 cm deterioration, and we see for 1 GeV electrons a decrease in this effect (recalling that position reconstruction alone improves with energy). These results are also supported with positron position reconstruction at the positron outside edge of the ECal.

5 Conclusions

In spite of a large range of energies and angles, adequate corrections could be found for improving energy and position reconstruction. All numerical results which would enter energy and position reconstruction are compiled in Table 1. They are valid excluding an edge of about 10 mm around all the physical edges of ECal, and can be used as such for the inital data analysis. A portion of this border could be recovered with more detailed studies.

The numerical values obtained here may have to be revisited before final data calibra-

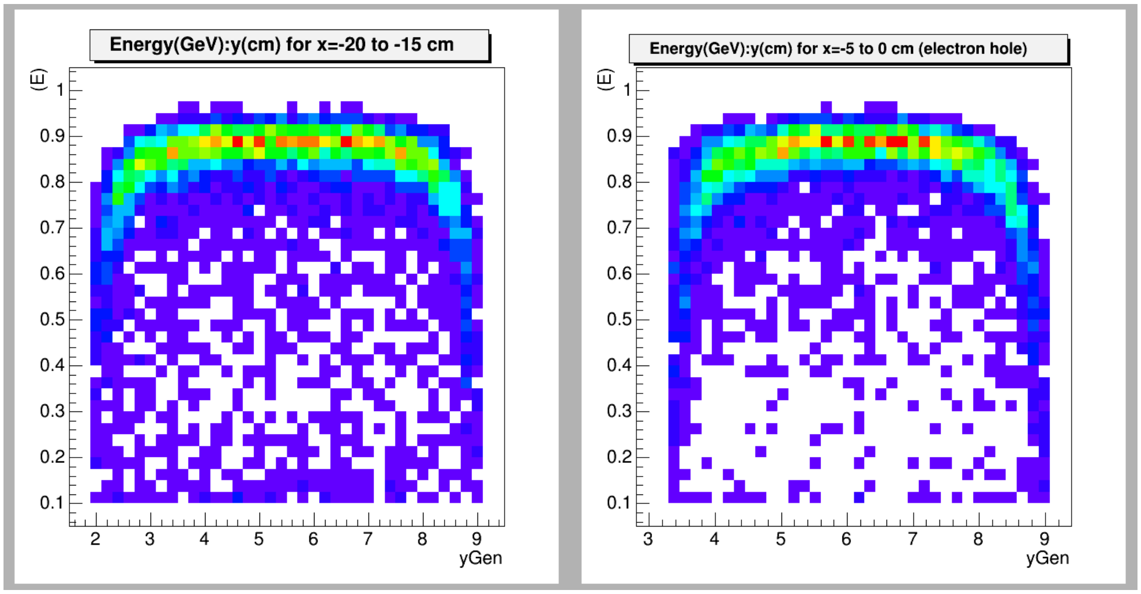

Figure 25: Sampling fraction as a function of vertical position for 1 GeV electrons at fixed x. The edges are at 2 and 9 cm.

tion and analyses, especially if the crystal energy threshold ends up being different from 7.5 MeV (or different from crystal to crystal). In this study, we do not claim a precision better than 1-2% for the sampling fraction. For a very precise calibration, one will have to take a closer look at the energy (and position) dependence of w_0, as well as at the position dependence of f. This will require larger statistics (about 10^4 particles per cm^2 on the calorimeter and per energy).

The energy resolution in the ECal is shown here to be an improvement over that specified in the HPS proposal due to electronic component upgrades. The implications of using the ECal position and energy measurements for the lepton track reconstruction are discussed in the Appendix.

Appendix: considerations on HPS resolutions

We reexamine here the main features of the lepton pair invariant mass resolution, in view of quantifying how much the ECal energy and position information could improve on this resolution.

Using a small angle approximation (the results hereafter do not depend on this approximation), the invariant mass is $M = \sqrt{E_1 E_2}\Theta$, where Θ is the opening angle between the two leptons. Neglecting at this stage the correlation between momentum and angle

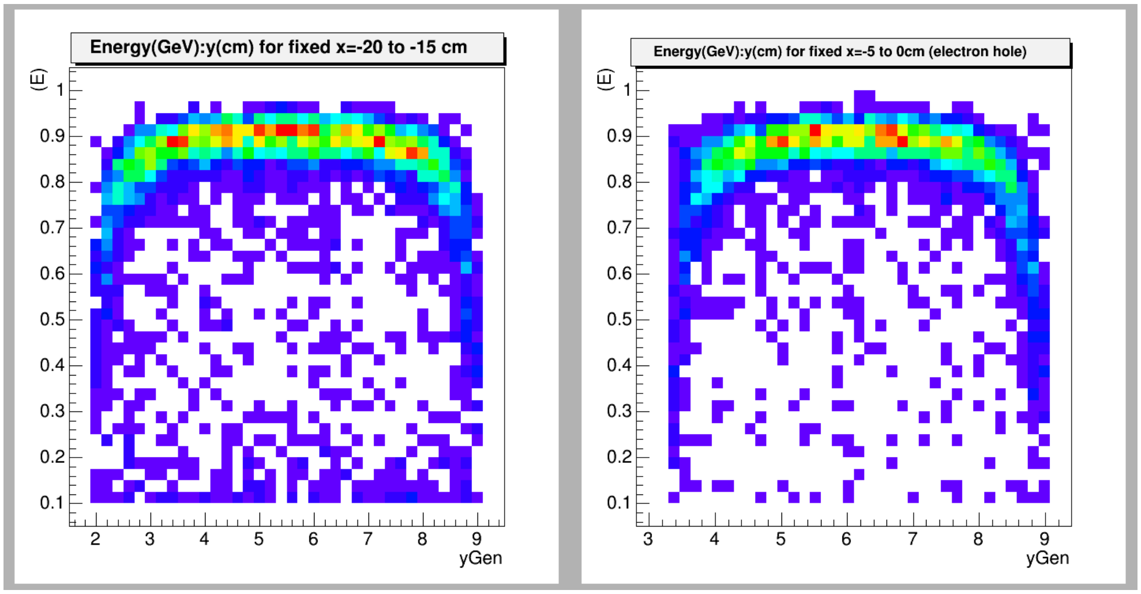

Figure 26: Sampling fraction as a function of vertical position for 1 GeV photons at fixed x. The edges are at 2 and 9 cm.

measurements, one gets:

$$\sigma_M = \frac{1}{\sqrt{2}} M \frac{\sigma_E}{E} \oplus \sqrt{E_1 E_2}\sigma_\Theta, \tag{7}$$

where we have only assumed that the energy resolution is the same for the two leptons, which is almost the case for the SVT determination of the momentum. For $E_1 \simeq E_2 \simeq E \simeq E_{\text{beam}}/2$, and in the worst case of lepton pair emitted close to the horizontal plane, where Θ is the difference between the two horizontal angles measured with a resolution σ_θ,

$$\sigma_M \simeq \frac{1}{\sqrt{2}} M \frac{\sigma_E}{E} \oplus \sqrt{2} E \sigma_\theta \tag{8}$$

which, for 1 GeV leptons, leads to

$$\sigma_M(\text{MeV}) \simeq 0.7 \times \frac{M\ (\text{MeV})}{100} \times \frac{\sigma_E}{E}\ (\%)\ \oplus\ 1.4 \times \sigma_\theta\ (\text{mrad}) \tag{9}$$

This result was checked with an ad-hoc simulation. The first term, proportional to M, is recovered exactly, while the second, independent of M, is slightly overestimated in Eq. 9. This is not surprising since we considered there lepton pairs emitted in the horizontal plane only. Setting a vertical angle resolution at about $\sigma_\theta/2$ [4], we find $\sigma_\Theta \simeq 1.2\sigma_\theta$, and we will use hereafter the corrected expression:

$$\sigma_M(\text{MeV}) \simeq 0.7 \times \frac{M\ (\text{MeV})}{100} \times \frac{\sigma_E}{E}\ (\%)\ \oplus\ 1.2 \times \sigma_\theta\ (\text{mrad}) \tag{10}$$

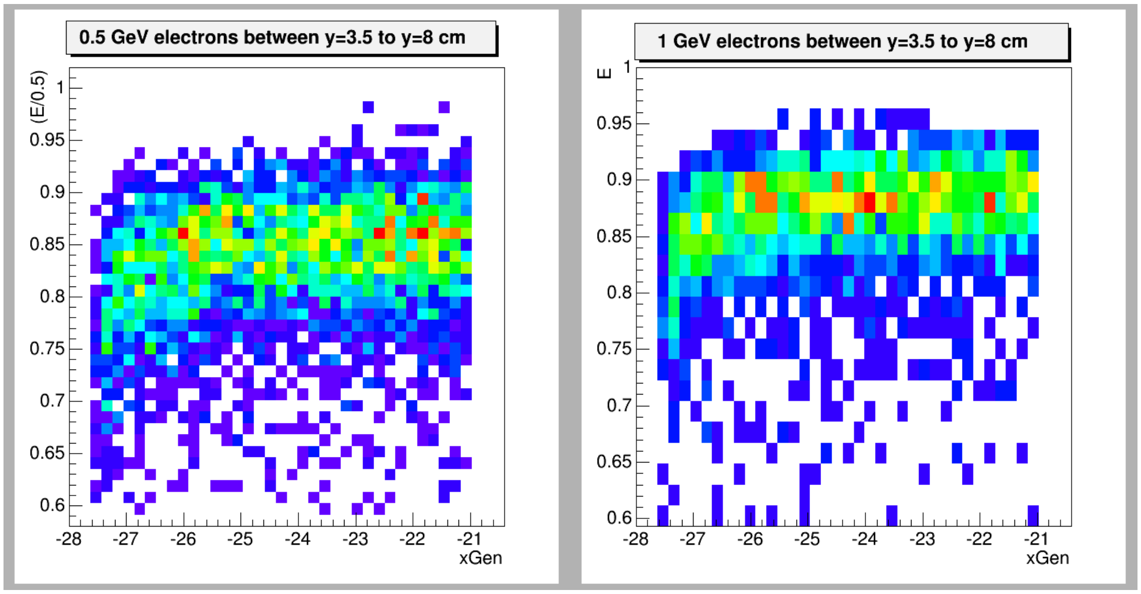

Figure 27: Sampling fraction as a function of horizontal position at fixed y, for 0.5 and 1 GeV electrons. The edge is at -27.5 cm.

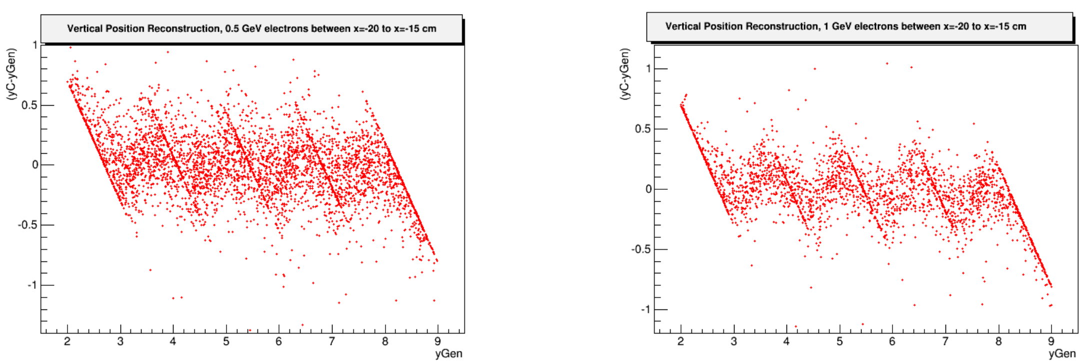

Figure 28: Position reconstruction near the outer edges of the ECal, at fixed x, for 0.5 and 1 GeV electrons. The edges are at 2 and 9 cm.

5.1 SVT alone

For a 4.5% momentum resolution (as in the proposal) and a 100 MeV mass, we find $\sigma_M > 3.2$ MeV, somewhat higher than in the proposal (2-2.5 MeV).

With the latest SVT reconstruction alogrithm, $\sigma_p/p \simeq 3\%$ [5] and $\sigma_\theta = 2.5$ mrad [4],

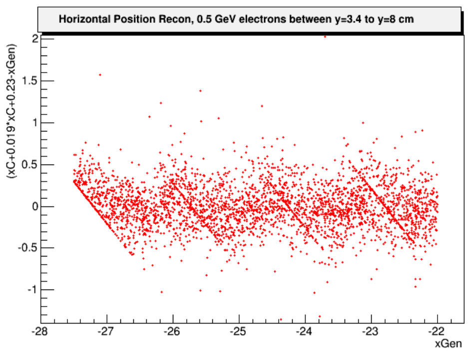

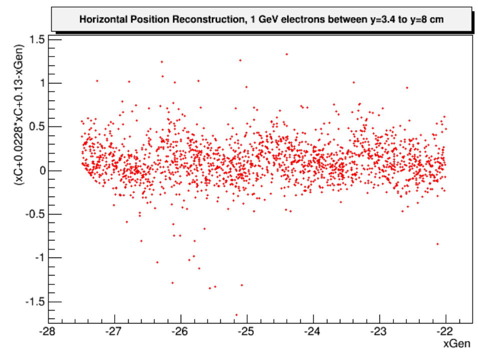

Figure 29: Position reconstruction near the outer edges of the ECal, at fixed y, for 0.5 and 1 GeV electrons. The edge is at -27.5 cm.

	f	w_0	A	B (cm)
e^-	$-0.0027E_{cl} - 0.06/\sqrt{E_{cl}} + 0.95$	3.1	$0.0066/\sqrt{E_{cl}} - 0.030$	$0.028E_{cl} - 0.451/\sqrt{E_{cl}} + 0.465$
e^+	$-0.0096E_{cl} - 0.042/\sqrt{E_{cl}} + 0.94$	3.1	$0.0072/\sqrt{E_{cl}} - 0.031$	$0.007E_{cl} + 0.342/\sqrt{E_{cl}} + 0.108$
γ	$0.0015E_{cl} - 0.047/\sqrt{E_{cl}} + 0.94$	3.1	$0.005/\sqrt{E_{cl}} - 0.032$	$0.011E_{cl} - 0.037/\sqrt{E_{cl}} + 0.294$

Table 1: Numerical values of parameters entering the energy and position reconstruction

we find $\sigma_M = 2.1 \oplus 3.0 = 3.7$ MeV.

5.2 SVT plus ECal energy

The combination of two independent measurements yield the resolution

$$\frac{\sigma_E}{E} = \left[\left(\frac{\sigma_p}{p}\right)^{-2}_{\text{SVT}} + \left(\frac{\sigma_E}{E}\right)^{-2}_{\text{ECal}}\right]^{-1/2}, \tag{11}$$

or $\sigma_E/E = 2.3\%$ so that the first term in σ_M changes from 2.1 to 1.6 MeV (still for 1 GeV leptons).

5.3 SVT plus ECal position

For a particle emitted at the target location in the horizontal plane with angle $dx/dz = x_0'$ ($\simeq \theta$) and energy/momentum E, we wrote the equation of the trajectory in the magnetic field (arc of circle) and then from the magnet to ECal (straight line). This results in an equation $x_{cal} = f(E, x'_0)$ which expresses the correlation between the measured coordinate on ECal, the energy (whether it is measured by SVT, ECal, or both), and the angle at target. This equation is not easily inverted, but it is sufficient for our purpose here to generate Figs 30 and 31 and infer graphically the derivatives of $dx/dz = x'_0$ with respect to E at constant x_{cal} and with respect to x_{cal} at constant E, following the "isochrome" lines on these plots:

$$\frac{\partial x'_0}{\partial E} = 100\,\text{mrad/GeV, or } E\frac{\partial x'_0}{\partial E} = 1\,\text{mrad/\%}\ \text{(at 1 GeV, nearly independent of position)}, \tag{12}$$

$$\frac{\partial x'_0}{\partial x_{cal}} = 0.7\ \text{mrad/mm}\ \ \text{(independent of energy and position)} \tag{13}$$

These numbers may also be calculated from first-order transport theory [6]. A simple

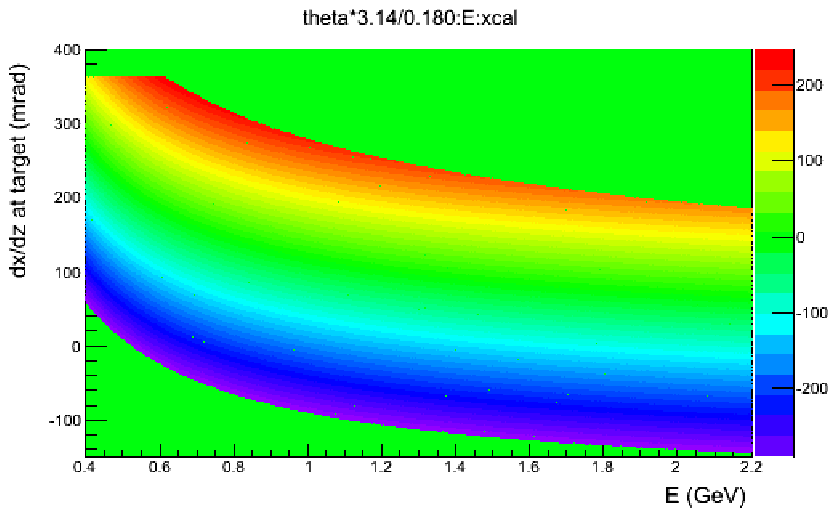

Figure 30: Horizontal angle at target vs energy, for different hit positions on ECal.

matrix algebra leads to

$$E\frac{\partial x'_0}{\partial E} = [\rho(1-\cos\alpha) + d\sin\alpha][\rho\sin\alpha + d\cos\alpha]^{-1}, \tag{14}$$

$$\frac{\partial x'_0}{\partial x_{cal}} = [\rho\sin\alpha + d\cos\alpha]^{-1}, \tag{15}$$

with ρ (radius of curvature) = 6.7 m, α (bend angle) = 8.6° and d (free field distance along trajectory between end of magnet and ECal) = 0.42 m. The numerical results are thus confirmed.

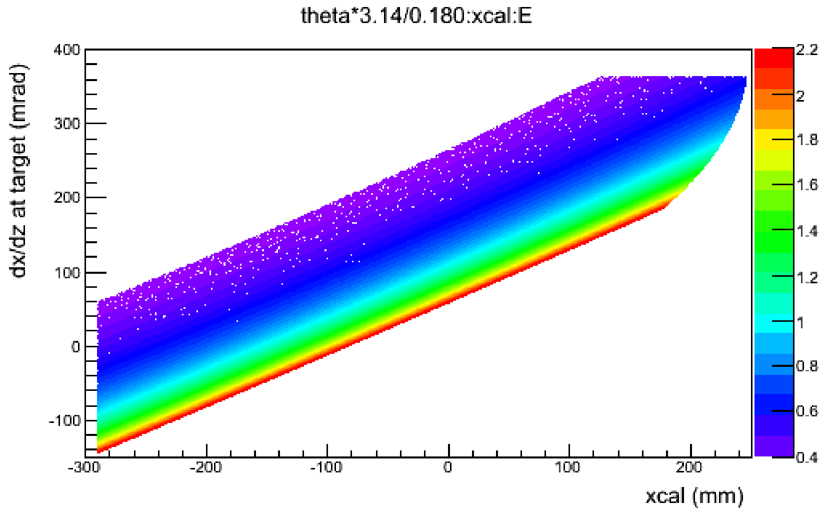

Figure 31: Horizontal angle at target vs hit position on ECal, for different energies

If the initial angle were to be reconstructed uniquely from energy (with resolution 2.3%) and ECal position (with 2 mm resolution), we would have, ignoring multiple scattering, $\sigma_\theta = 2.3 \oplus 1.4$ mrad. These numbers are comparable, or not much larger, than expected from SVT alone. It means that taking into account the ECal position in the tracking algorithm would improve the angle determination, and thus the missing mass resolution. It is beyond the scope of this Note to complete the exercise with a tracking algorithm, but we would suggest that an option be added to the SVT tracking to incorporate the ECal hit position as a seventh measurement along the lepton tracks (after track-cluster matching and particle identification).

References

[1] R. Niyazov and S. Stepanyan, CLAS-Note 2005-007.

[2] F.-X. Girod and M. Garçon, CLAS-Note 2005-001.

[3] R. Niyazov and S. Stepanyan, CLAS-Note 2005-021.

[4] M. Graham, HPS DOE review, July 2013, slide 8. Note that the formulae on invariant mass (misprint) and its error are not correct on this slide.

[5] M. Graham, June 2014 HPS colllaboration meeting, slide 5.

[6] K.L. Brown, SLAC report, 1975.